Predictive Control of Low-Cost Three-Phase Four-Switch Inverter-Fed Drives for Brushless DC Motor Applications

Naseri, Farshid; Farjah, Ebrahim; Schaltz, Erik; Lu, Kaiyuan; Tashakor, Nima

Published in:
IEEE Transactions on Circuits and Systems I: Regular Papers

DOI (link to publication from Publisher):
10.1109/TCSI.2020.3043468

Publication date:
2021

Document Version
Accepted author manuscript, peer reviewed version

Predictive Control of Low-Cost Three-Phase Four-Switch Inverter-Fed Drives for Brushless DC Motor Applications

Farshid Naseri, *Member, IEEE*, Ebrahim Farjah, *Member, IEEE*, Erik Schaltz, *Member, IEEE*, Kaiyuan Lu, *Member, IEEE*, and Nima Tashakor, *Graduate Student Member, IEEE*

***Abstract*— In this paper, an efficient control strategy for three-phase four-switch inverter-fed Brushless DC Motor (BLDCM) drives with trapezoidal back Electromotive Force (EMF) is proposed. In the proposed approach, the outer control loop for adjusting the motor speed is designed using Model Predictive Control (MPC) while the inner control loop based on a hysteresis controller regulates the BLDC phase currents. To effectively adjust the current of the uncontrolled phase in the four-switch inverter, efficient switching strategies for motor and generator modes are suggested. The proposed control scheme achieves favorably low torque ripples and improves the speed transient response in terms of tracking error and speed overshoot/undershoot. Therefore, it can be an ideal candidate for low-cost low-power BLDCM applications. Also, the MPC-based speed control loop is tuned by solving a suitable cost function in an offline manner to minimize the real-time computational effort. Using the foregoing technique, it is shown that the implementation of the proposed MPC-based controller becomes as simple as the PI controller while the MPC-based controller achieves superior control performance. The proposed BLDCM drive scheme is experimentally verified in a Hardware-in-the-Loop (HiL) test setup with a 1200W BLDCM and dSPACE1104 development board. The experimental results demonstrate the benefits of the proposed drive system.**

***Index Terms*— Hysteresis control, brushless DC motor (BLDCM), four-switch inverter-fed motor drives, Hardware-in-the-Loop, model predictive control.**

I. Introduction

BRUSHLESS DC Motors (BLDCMs) have come to dominate a wide range of applications including household appliances, small electric bikes, motion control systems, etc. [1], [2]. The superiorities of the BLDCMs mainly include higher power density, higher efficiency, and longevity of these machines compared to their brushed counterparts. The common method for driving the three-phase BLDCMs is to use three-phase Six-Switch Voltage Source Inverters (SSVSIs) [3]. Alternatively, three-phase Four-Switch Voltage Source Inverters (FSVSIs) with special control mechanisms have been used to drive the BLDCMs [4]–[18]. In the FSVSI, one leg of the three-phase SSVSI is substituted by two common series-connected capacitors and one motor terminal is connected to the center tap of these capacitors. Thus, due to the elimination of two semiconductor switches and related gate drive circuitry, the overall implementation cost would be reduced, which makes the FSVSI a favorable choice for low-power BLDCM drives. Nonetheless, in the FSVSI-based BLDCM drive, one of the phases becomes uncontrollable which may lead to fluctuations in the center tap voltage of the capacitors and unbalance among the BLDCM phase currents. Such conditions can potentially increase the torque ripples and in the worst case lead to a failure in the drive system. Therefore, for FSVSI-based BLDCM drives, it is necessary to adopt efficient control strategies for minimizing the torque ripple and ensuring that the speed/current transient responses are not too harsh to cause control loop instability and damage to the weak FSVSI system. To this end, several approaches have been proposed in the literature, which all are briefly reviewed in the following:

The feasibility of using FSVSI for low-cost BLDCM drives was first evaluated by Lee and Ehsani in [4]–[6], where direct current controlled pulse wide modulation (PWM) was used together with an efficient switching strategy for minimizing the torque ripple of the BLDCM. Several other research works have so far been proposed for controlling the FSVSI-fed BLDCMs. In [7], an effective compensation scheme for reducing the current imbalance caused by the capacitive impedances of the uncontrolled phase of the FSVSI-fed motor drives has been proposed. The main idea of this work is to add similar virtual capacitive impedances to the terminals of the controlled phases for balancing the three-phase system. In [8], a current reference generation scheme has been proposed for space vector PWM (SVPWM)-based FSVSI-fed BLDCM drives to reduce the torque ripple during current commutations. In [9], a comprehensive analysis of low-frequency and high-frequency torque ripples in the SVPWM-based FSVSI-fed drives has been carried out. Additionally, a simple compensation scheme based on the introduction of non-orthogonal

Manuscript received May 1, 2020; revised November 10, 2020; accepted December 4, 2020. This work was supported by the Irans National Elites Foundation. This article was recommended by Associate Editor T. Fernando. *(Corresponding author: Ebrahim Farjah.)*

Farshid Naseri and Ebrahim Farjah are with the Advanced Power Electronics and Electric Vehicle Laboratory, Shiraz University, Shiraz 71348-51154, Iran (e-mail: f.naseri@shirazu.ac.ir; farjah@shirazu.ac.ir).

Erik Schaltz and Kaiyuan Lu are with the Department of Energy Technology, Aalborg University, 9220 Aalborg, Denmark (e-mail: esc@et.aau.dk; klu@et.aau.dk).

Nima Tashakor is with the Department of Electrical and Computer Engineering, Technical University of Kaiserslautern, 67663 Kaiserslautern, Germany (e-mail: tashakor@eit.uni-kl.de).

Color versions of one or more figures in this article are available at https://doi.org/10.1109/TCSI.2020.3043468.

Digital Object Identifier 10.1109/TCSI.2020.3043468

coordinate transformation has also been proposed to minimize the torque ripples. Minimization of the torque ripples in FSVSI-fed drives has also been discussed in [10], where a hybrid SVPWM method based on using two zero vector synthesis approaches during each fundamental period has been proposed. In [11], two SVPWM approaches for the FSVSI-fed drives have been proposed to suppress the zero-sequence voltage/current. In the current control scheme proposed in [12], two regulating vectors have been added to each control cycle of the conventional PWM scheme for regulating the current of the uncontrolled phase by controlling the activation time of the regulating vectors. The application of the direct torque control (DTC) for BLDCMs driven with FSVSI has been proposed in [13]. In this work, the required quasi-square current waveforms are obtained by selecting the voltage space vectors from a simple look-up table at a predefined sampling time. Additionally, an efficient switching template based on the voltage vector look-up table has been proposed to produce the desirable torque characteristics. To further improve the cost-effectiveness of the FSVSI-fed BLDCM drives, an effective control strategy that uses only one current sensor has been proposed in [14]. In the control scheme proposed in [14], only the current waveform of the uncontrolled phase is measured and directly used to control the respective phase current during its activation periods. When the uncontrolled phase is at rest, the current regulation is accomplished by analytically deriving different rules that affect the uncontrolled phase current during the rest periods. To further reduce the implementation cost of the FSVSI-fed BLDCM drive, the feasibility of eliminating the Hall effect sensors by using sensorless control techniques have also been successfully verified in [15]–[17]. In all the control schemes reviewed before, simple PI controllers have been used to control the speed of the FSVSI-fed BLDCM. However, the use of the PI controller is not efficient especially in FSVSI-based applications where an aggressive speed transient response can cause intolerable transient conditions for the weak FSVSI-based drive. Therefore, apart from efficient control of the current loop, the speed control loop should also have a good performance. To achieve this goal, in [18], the fuzzy logic-based controller has been proposed to adjust the speed of the motor equipped with FSVSI, where excellent performance characteristics in terms of the speed overshoot/undershoot and steady-state tracking error have been obtained. However, it is often tedious to develop the required fuzzy rules and membership functions. Also, developing a fuzzy system requires a lot of data and expertise.

The usefulness of Model Predictive Control (MPC) for controlling FSVSI-based Permanent Magnet Synchronous Motor (PMSM) drives have been discussed in [19], [20]. In [19], a simplified MPC without weighting factors is formulated to control the motor flux, where the capacitor voltage offset is also suppressed using a stator flux compensator. The MPC-based flux control of FSVSI-based flux-reversal permanent magnet (FRPM) motor drives has also been discussed in [20]. However, in these works, the MPC has been used for controlling the motor flux and the speed loop is adjusted using the traditional PI controllers. In this paper, an efficient control strategy for FSVSI-fed BLDCMs is proposed. In the proposed control scheme, the outer speed control loop is realized using Model Predictive Control (MPC), which helps to achieve a superior speed transient response. The MPC generates optimum references for the motor phase currents, which are subsequently fed to the inner current control loop based on the hysteresis control mechanism. Besides, efficient switching patterns for current control at both motor and generator modes are developed, which substantially reduce the BLDCM torque ripple during motor and generator modes. The contributions of this paper are explicitly listed as follows:

1- This work is the first attempt for predictive speed control of the FSVSI-fed BLDCMs. In comparison with the existing methods, The proposed scheme provides a superior speed transient response.
2- The control law of the proposed MPC controller is obtained in an offline manner, which significantly improves the computational efficiency. It is also mathematically shown that the implementation of the proposed MPC controller becomes as simple as a PI controller.
3- In comparison with other methods that discuss only the motor mode, the switching patterns and current control for the generator mode are developed, as well.

The rest of the paper is structured as follows. In Section II, the problem of controlling the BLDCM with FSVSI structure is discussed in more detail. In Section III, the operating principles of the proposed approach including the MPC-based speed controller, switching patterns, and hysteresis current controller are discussed. To demonstrate the effectiveness of the proposed control scheme, the HiL experimental results are provided and discussed in Section IV. Section V provides comparative results between the proposed method and some other approaches. Finally, in Section VI, the concluding remarks are provided.

II. FSVSI-Based BLDCM Control: Problem Statement

As shown in Fig. 1, the BLDCM produces trapezoidal back-Electromotive Force (EMF). Therefore, to generate constant output torque, the motor phase currents must necessarily have quasi-square waveforms synchronized with the three-phase back-EMFs. To achieve this, the phase currents must have 120° conducting and 60° non-conducting working regions during each half cycle of the motor electrical frequency. Likewise, at each instant, only two motor phases are active and the third phase current is zero. The required waveforms for proper operation of the BLDCM during motor and generator operation modes are shown in Fig. 1. The waveforms of Fig. 1 can be straightforwardly realized using the SSVSI structure with conventional PWM strategies. However, obtaining the quasi-square current waveforms of Fig. 1 using the FSVSI topology is challenging. The structure of the FSVSI-fed BLDCM is depicted in Fig. 2. As seen, since in the FSVSI two power switches are replaced by two capacitors, Phase C current can no longer be directly controlled. Taking the motor operation mode (upper figure of Fig. 1) as an example, in operating modes 1, 3, 4, and 6, Phase C current can be indirectly controlled by appropriate switching of S_4,

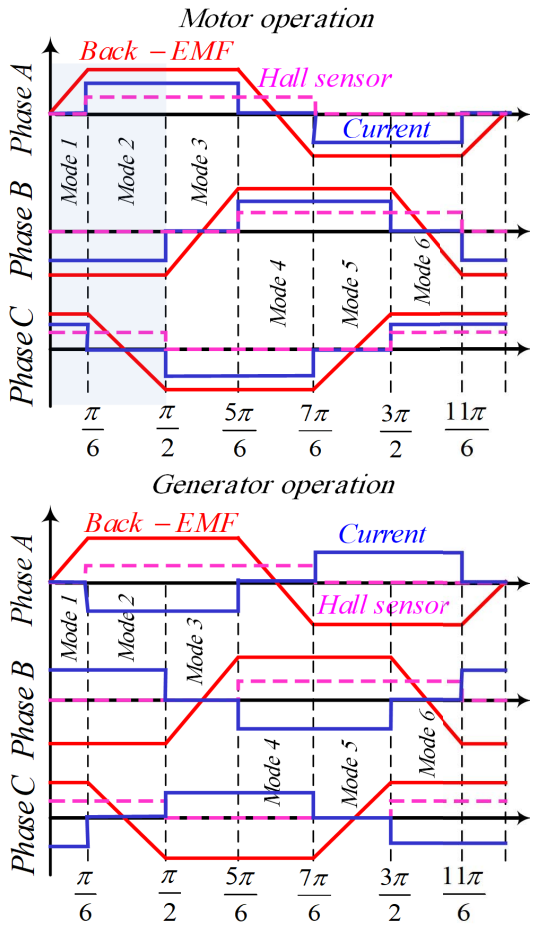

Fig. 1. Three-phase back-EMFs, current waveforms, and Hall effect signals of the BLDCM during one cycle of the motor electrical frequency under motor and generator operating modes.

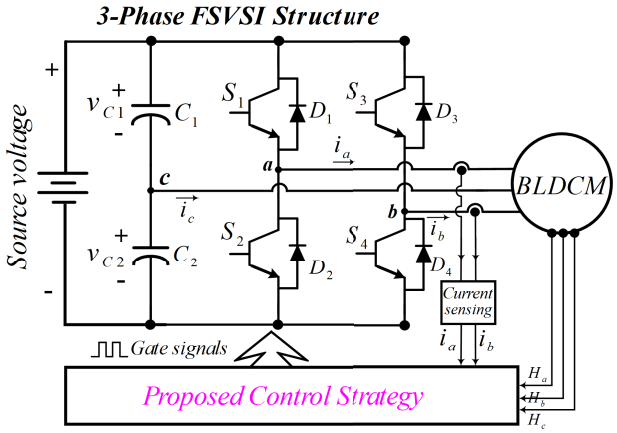

Fig. 2. Schematic of the FSVSI-fed BLDCM.

S_1, S_3, and S_2, respectively. However, during the operating modes 2 and 5, Phase C current cannot be set to zero with the traditional PWM strategy due to the fluctuations of the center tap voltage of the capacitors. Thus, during the rest periods related to modes 2 and 5, Phase C current continues to flow, which causes current imbalance and torque pulsation. Thus, an efficient control scheme must be adopted to rectify the problem associated with the uncontrolled Phase C.

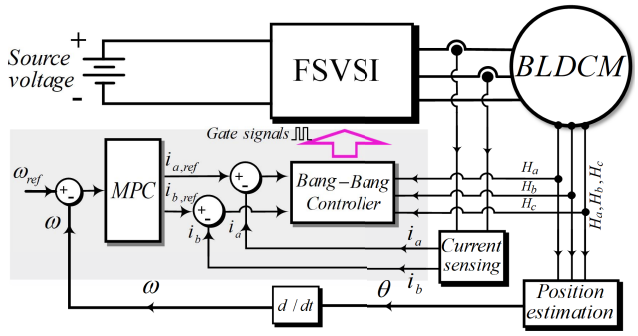

Fig. 3. Overview of the proposed control strategy for FSVSI-fed BLDCM.

Under the conditions explained above, the proper operation of the outer speed control loop also gains more importance because harsh transient responses might aggravate the voltage variations at the midpoint of the capacitors leading to instability of the speed control loop [21]. In the next section, and efficient strategy for FSVSI-fed BLDCM control is proposed.

III. Operating Principles of the Proposed Control Scheme

The structure of the proposed control scheme for the FSVSI-fed BLDCM is shown in Fig. 3, in which the gate signals of the FSVSI are considered as the control variables and speed of the BLDC motor is considered as the controlled variable. The motor speed is estimated using the low-resolution Hall effect sensors H_a, H_b, and H_c. As seen in Fig. 1, the status of Hall signals overall change six times (with $\pi/3$ phase shift) during each cycle of the motor electrical frequency. Thus, the motor speed can be easily estimated as follows:

$$\omega = \frac{\pi/3}{\Delta t} \times \frac{2}{P} = \frac{2\pi}{3P\Delta t} \tag{1}$$

where ω is the motor speed in *rad/s*, P is the number of poles, and Δt is the measured time interval of $\pi/3$ periods. The motor speed ω is compared to its reference value ω_{ref} ($\bar{\omega}$) and the control error is fed to the speed controller. In the proposed control scheme, the MPC controller is used for realizing the outer control loop (speed loop). The speed control loop generates suitable references $i_{a,ref}$ and $i_{b,ref}$ for the controllable motor phase currents. Besides, the current regulation is realized using an inner control loop based on the hysteresis controller together with efficient switching templates for motor and generator operation modes. As will be demonstrated, the proposed control scheme provides superior transient response during speed or torque changes. Also, similar to conventional control methods, the proposed method uses two current sensors and three built-in Hall effect sensor signals, and thus, no hardware extension is required. The detailed procedure for designing the speed and current control loops are provided in the following subsections.

A. Design of the MPC-Based Speed Control Loop

It is well-known that the hysteresis controller has a very fast response. Also, the electrical time constant of the BLDCM

is usually much lower than the mechanical time constant. Therefore, it can be assumed that the bandwidth of the current control loop is wider than the speed control loop, which means that the current control loop will have sufficient time to track the set of reference current signals produced by the speed controller. In this paper, the MPC controller is adopted for regulating the BLDCM speed. The MPC is an optimum model-based control approach, in which the control commands are decided by minimizing a Cost Function (CF) to provide the best reference tracking performance. Given these facts and considering that the input and output of the MPC controller are the speed error of the BLDC motor and the reference current signals, respectively, the required MPC model can be considered as follows:

$$T_e - T_L = J\frac{d\omega}{dt} + B\omega \tag{2}$$

where T_e is the electromagnetic torque, T_L is the load torque, J is the moment of inertia, and B is the damping coefficient. Equation (2) can be discretized as follows:

$$K_T I(k-1) - T_L = J\frac{1-z^{-1}}{T_s}\omega(k) + B\omega(k) \tag{3}$$

Equation (3) is obtained by substituting $T_e = K_T I$ in (2), where K_T is the torque constant. Likewise, T_s is the sampling time of the MPC controller, k is the time index, and z^{-1} is the unit back-shift operator. From (3), the Controller Auto-Regressive Moving-Average (CARMA) model for MPC design can be inferred as follows:

$$\underbrace{\left(J + BT_s - Jz^{-1}\right)}_{A(z^{-1})}\omega(k) = \underbrace{K_T T_s}_{B(z^{-1})} I(k-1) \underbrace{-T_s}_{C(z^{-1})} T_L \tag{4}$$

where $A(z^{-1})$, $B(z^{-1})$, and $C(z^{-1})$ are z-polynomials as follows:

$$\begin{aligned} A(z^{-1}) &= J + BT_s - Jz^{-1} = a_0 + a_1 z^{-1} \\ B(z^{-1}) &= K_T T_s = b_0 \\ C(z^{-1}) &= -T_s = d_0 \end{aligned} \tag{5}$$

In the MPC controller, the control variable (output of the MPC controller) is obtained solving the following CF:

$$CF = \sum_{j=1}^{N_p} \delta\left[\hat{\omega}(k+j\,|\,k) - \bar{\omega}(k+j)\right]^2 + \sum_{j=1}^{N_c} \lambda\left[\Delta I(k+j-1)\right]^2 \tag{6}$$

where N_p is the prediction horizon, N_c is the control horizon, δ and λ are appropriate output and control weighting factors, respectively, ΔI is the required control effort (reference current commands), and $\bar{\omega}$ is the reference speed. The weighting factors determine the relative importance of the prediction and control terms in the CF [22]. Also, $\hat{\omega}(k+j|k)$ denotes the prediction of speed at the instant $k+j$ on the premise that the information of ω up to the instant k is available. In the CF of (6), the prediction equations of the motor speed for $1 \le j \le N_p$ must be mathematically driven. The required prediction equations can be obtained using the well-known Diophantine equation [3]. The diophantine equation can be defined as follows:

$$1 = E_j(z^{-1})\tilde{A}(z^{-1}) + z^{-j}F_j(z^{-1}) \tag{7}$$

where $\tilde{A}\left(z^{-1}\right) = \Delta A(z^{-1})$ and $\Delta = 1 - z^{-1}$. The z-polynomials $E_j(z^{-1})$ and $F_j(z^{-1})$ can be uniquely defined with degrees of j-1 and 1 (the same degree of polynomial $A(z^{-1})$) and can be obtained through dividing 1 by $\tilde{A}\left(z^{-1}\right)$ until the remainder can be factorized in the form of $z^{-j}F_j(z^{-1})$ [3]. The quotient of this division is equal to the z-polynomial $E_j\left(z^{-1}\right)$. Upon determination of $E_j(z^{-1})$ and $F_j(z^{-1})$, the predictor equations can be obtained considering (7) and multiplying (4) by $\Delta E_j(z^{-1})z^j$ as follows:

$$\begin{aligned} &z^j \overbrace{E_j(z^{-1})\underbrace{\Delta A(z^{-1})}_{\tilde{A}(z^{-1})}}^{(1-z^{-j}F_j(z^{-1}))}\omega(k) \\ &= \Delta E_j(z^{-1})z^j B(z^{-1})I(k-1) \\ &\quad + \Delta E_j(z^{-1})z^j C(z^{-1})T_L \Rightarrow \omega(k+j) = F_j(z^{-1})\omega(k) \\ &\quad + E_j(z^{-1})B(z^{-1})\Delta I(k+j-1) \\ &\quad + E_j(z^{-1})C(z^{-1})\Delta T_L(k+j) \end{aligned} \tag{8}$$

From (8), the expected value of $\omega(k+j)$ can be derived as follows:

$$\begin{aligned} \hat{\omega}(k+j|k) = E[\omega(k+j)] &= F_j(z^{-1})\omega(k) \\ &\quad + E_j(z^{-1})B(z^{-1})\Delta I(k+j-1) \end{aligned} \tag{9}$$

where $E[]$ denotes the expected value. The j-step-ahead prediction equation of (9) should be substituted in the CF of (6) for solving the optimization problem and to obtain the optimum control action. Considering a prediction horizon of 2 ($N_p = 2$), the one-step-ahead ($\hat{\omega}(k+1|k)$) and two-step-ahead ($\hat{\omega}(k+2|k)$) prediction equations should be obtained solving Diophantine equation of (7) and substituting the obtained polynomials $E_1(z^{-1})$, $F_1(z^{-1})$, $E_2(z^{-1})$, and $F_2(z^{-1})$ in (9). The one-step-ahead predictor equation $\hat{\omega}(k+1|k)$ is obtained as follows:

$$\hat{\omega}(k+1|k) = \underbrace{\left(\frac{a_0 - a_1}{a_0} + \frac{a_1}{a_0}z^{-1}\right)}_{F_1(z^{-1})}\omega(k) + \underbrace{\frac{1}{a_a}}_{E_1(z^{-1})} b_0\Delta I(k) \tag{10}$$

The two-step-ahead predictor equation $\hat{\omega}(k+2|k)$ is also obtained as follows:

$$\begin{aligned} \hat{\omega}(k+2|k) = &\underbrace{\left[\left(\frac{a_1}{a_0} + \frac{(a_1-a_0)^2}{a_0^2}\right) + \frac{a_1(a_0-a_1)}{a_0^2}z^{-1}\right]}_{F_2(z^{-1})}\omega(k) \\ &+ \underbrace{\left(\frac{1}{a_0} + \frac{(a_0-a_1)}{a_0^2}z^{-1}\right)}_{E_2(z^{-1})} b_0\Delta I(k+1) \end{aligned} \tag{11}$$

where the coefficients of the z-polynomials $A(z^{-1})$ and $B(z^{-1})$ can be inferred from (4) and (5).

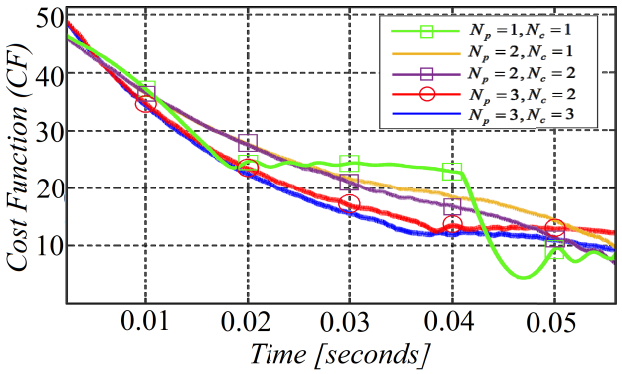

Fig. 4. The MPC cost function plotted for different values of prediction and control horizons.

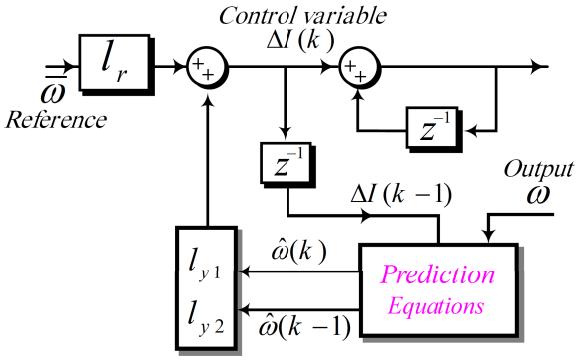

Fig. 5. Block diagram of the proposed MPC-based speed controller for the FSVSI-fed BLDCM (this structure shows details of the "MPC" block in Fig. 3).

Generally, selecting larger prediction and control horizons may lead to a better control system performance at the cost of a higher computational burden. In practice, there should be a trade-off between the required control performance and computational cost. It should also be considered that the control horizon should always be shorter than the prediction horizon [3]. The common practice for selecting the MPC horizons has been the trial and error approach, which is adopted in this study too [22], [23]. In Fig. 4, some offline case studies of the CF of the MPC controller for different values of the prediction and control horizons are shown. The CFs of Fig. 4 are obtained assuming that the BLDC motor experiences a stepwise change in the reference speed from standstill condition to 1000 rpm. While the results approve the correctness of the aforementioned statements, it is observable that increasing the prediction horizon above 2 will not lead to a significant reduction of the cost function. However, increasing the MPC horizons substantially increases the computational load, which will increase the cost of embedded implementation. Given these facts and because the main target of this work is to achieve a cost-effective solution for BLDC motor drive, the prediction and control horizons are selected as follows:

$$N_p = 2, \quad N_c = 1$$

It should be noted that the horizons of the MPC controller can also be selected based on other authentic methods such as the genetic or butterfly optimization algorithms [24], [25]. To further reduce the real-time computational effort of the proposed MPC-based speed controller, the CF of (6) is solved in an offline manner to derive the required control action $\Delta I(k)$. To this end, the derivative of CF with respect to $\Delta I(k)$ must be set equal to zero. Accordingly, the optimum value of $\Delta I(k)$ is obtained as follows:

$$\Delta I(k)\overbrace{\left(2\delta\left(\frac{b_0}{a_0}\right)^2+2\lambda\right)}^{K} = -2\delta\left(\frac{a_0-a_1}{a_0}+\frac{a_1}{a_0}z^{-1}\right)\frac{b_0}{a_0}\hat{\omega}(k)+2\delta\bar{\omega}\left(\frac{b_0}{a_0}\right) \quad (12)$$

The control action $\Delta I(k)$ can be rewritten in the following form:

$$\Delta I(k) = \overbrace{\frac{-2\delta b_0(a_0-a_1)}{Ka_0^2}}^{l_{y1}}\hat{\omega}(k)+\overbrace{\frac{-2\delta b_0 a_1}{a_0^2 K}}^{l_{y2}}\hat{\omega}(k-1) + \underbrace{\frac{2\delta b_0}{a_0 K}}_{l_r}\bar{\omega} = l_{y1}\hat{\omega}(k)+l_{y2}\hat{\omega}(k-1)+l_r\bar{\omega} \quad (13)$$

Based on (13), the MPC-based controller coefficients l_{y1}, l_{y2}, and l_r can be easily tuned using some parameters of the BLDCM as well as the weighting factors. Using the trial and error approach, the weighting factors δ and λ are set to 0.7 and 0.3, respectively. The diagram of the proposed control scheme is shown in Fig. 5. The proposed MPC-based controller has a negligible computational effort since no CF needs to be solved in real-time. As will be discussed in the results section (Section IV), the designed speed controller outperforms the conventional PI controller in terms of transient response and steady-state tracking error. The generated reference current commands by the proposed MPC-based speed controller are then fed to the hysteresis controller for adjusting the motor phase currents. The hysteresis controller principles are fully discussed in the next subsection.

B. Design of the Current Control Loop Based on Hysteresis Controller

As discussed, utilization of the current controller with the conventional PWM strategy is not possible in the FSVSI-based BLDCM drive structure due to the undesirable torque pulsations caused by the uncontrolled Phase C. To overcome this problem, in this work, the hysteresis controller together with efficient switching patterns are used for regulation of the phase currents during both motor and generator operating modes. The switching patterns during the motor and generator operation modes are shown in Table I. The hysteresis controller is adopted for the inner current control loop due to its fast dynamic response, which is essential for the implementation of the switching templates as well as for real-time compatibility. In the proposed control design, the speed

TABLE I
SWITCHING PATTERNS FOR CURRENT REGULATION USING THE FSVSI

Mode*	$H_aH_bH_c$	Active Phases	Silent Phase	Switches (motor)	Switches (generator)
1	001	B, C	A	S_4	S_3
2	101	A, B	C	S_1 and S_4	S_2 and S_3
3	100	A, C	B	S_1	S_2
4	110	B, C	A	S_3	S_4
5	010	A, B	C	S_2 and S_3	S_1 and S_4
6	011	A, C	B	S_2	S_1

*Operating modes are depicted in Fig. 1

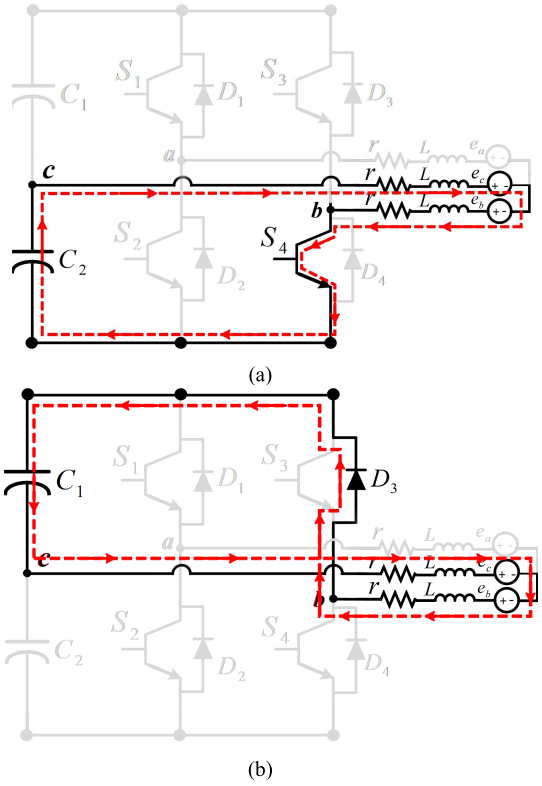

Fig. 6. Current flow during mode 1 of the utilized hysteresis current controller (motor operation). (a) S_4 is turned on and D_3 is deactivated (b) S_4 is turned off and D_3 is activated.

control loop generates the reference currents for the inner current control loop. The use of the fast hysteresis controller thus helps to finish the inner control objective before the next control input generated by the outer loop is received at the next sample time. With hysteresis controller, smaller overshoots/undershoots can also be achieved, which reduces the torque ripples of the motor.

Due to the space limitation, the operating modes 1 and 2 (refer to Fig. 1) during the motor mode are considered as examples to explain the working principles with more details. Assume I_{ref} and ε being the reference current command generated by the proposed MPC-based speed control loop and the hysteresis controller band, respectively. In mode 1 of the motor operation mode, switch A is deactivated making Phase A current equal to zero ($I_a = 0$). In this mode, the currents of active Phases B and C are controlled by switching of S_4. It should be noted that in this mode, as seen in Fig. 1, Phases B

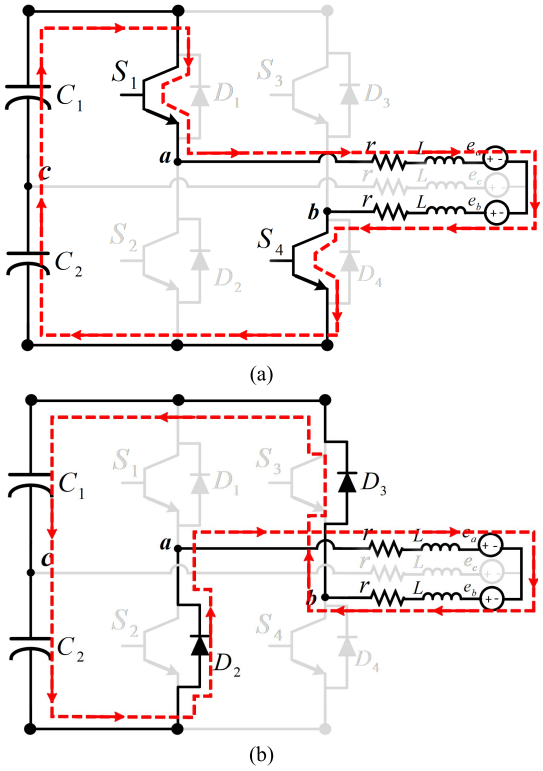

Fig. 7. Current flow during mode 2 of the utilized hysteresis current controller (motor operation). (a) S_1 and S_4 are turned on (b) S_1 and S_4 are turned off and current flow is automatically directed toward D_2 and D_3.

and C have negative and positive current values, respectively, i.e. $I_b < 0$, $I_c > 0$. Whenever $I_b > -I_{ref} - \varepsilon$ and $I_c < I_{ref} + \varepsilon$ the currents of Phases B and C should be increased to the reference current command. To this end, switch S_4 is turned on by the hysteresis controller. Fig. 6(a) shows the current paths in the FSVSI in this situation. As seen, when S_4 is turned on, the currents of Phases B and C are increased as a result of discharging capacitor C_2. The absolute phase currents steadily increase until the conditions $I_b \leq -I_{ref} - \varepsilon$ and $I_c \geq I_{ref} + \varepsilon$ are satisfied. As soon as the foregoing conditions are met, switch S_4 is turned off, which puts D_3 in the forward bias state and thus, the phase currents are reduced through charging capacitor C_1, as seen in Fig. 6(b). The foregoing procedure is repeated during each operating mode to maintain the phase current within the hysteresis control band. The same principle of mode 1 can be used for other operating modes. In mode 2, Phases A and B are active ($I_a > 0$, $I_b < 0$) and Phase C is silent ($I_c = 0$). Whenever $I_a < I_{ref} + \varepsilon$ and $I_b > -I_{ref} - \varepsilon$, power switches S_1 and S_4 are turned on to increase the phase currents by discharging the split capacitors C_1 and C_2 to Phases A and B windings, as depicted in Fig. 7(a). The absolute values of the currents I_a and I_b continue to increase until the phase currents I_a and I_b reach the upper and lower limits of the control band, respectively, i.e. when $I_a = I_{ref} + \varepsilon$ and $I_b = -I_{ref} - \varepsilon$. Then, the switches S_1 and S_4 are turned off, which diverts the paths of the phase currents to D_2 and D_3. Under such circumstances, as seen in Fig. 7(b), the magnitudes of the phase currents are reduced through charging the capacitors C_1 and C_2. Consequently, by

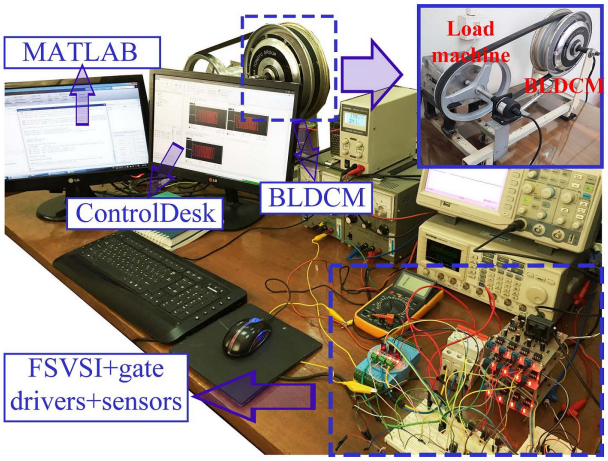

Fig. 8. Implemented HiL test setup.

turning on and off the switches S_1 and S_4, the increase and decrease of the phase currents can be controlled, which makes it possible to regulate the phase currents within a small control band around the reference current trajectory.

It should be mentioned that a smaller control band ε reduces the torque pulsations. However, if the control band is too small, the switching frequency increases, which gives rise to the switching losses. Thus, the selection of the control band in the utilized hysteresis controller should be made by a trade-off between the levels of the torque ripple and switching losses. With regards to the control modes 2 and 5, it should also be noted that the current of the uncontrolled Phase C might become nonzero (due to the non-zero back-EMF of Phase C and absence of the controllable power switches) and cause unwanted current distortions. To resolve this problem, the switching of the power switches is fulfilled, independently [6]. Therefore, the hysteresis controller is independently implemented for each operating mode of Table I. The active operating mode can easily be decided by monitoring of Hall effect sensors $H_aH_bH_c$, which have a unique status during each operating mode, as shown in the second column of Table I.

IV. Hardware-In-The-Loop Test Results and Discussions

To evaluate the performance of the proposed approach, several experiments are conducted on the implemented HiL test setup and the obtained results are provided and discussed in this section. In the following, the implemented HiL setup and the experimental results are discussed with details.

A. Description of the HiL Test Setup

The implemented Hil test setup is shown in Fig. 8. The HiL setup mainly comprises a motor-generator set equipped with a 1.2kW BLDCM coupled with a 1.5kW Permanent Magnet Synchronous Motor (PMSM) using a coupling belt with almost 1:1 speed ratio. Therefore, since the rating of the loading machine is higher than the under-study BLDC motor, the test motor can be loaded to its rated torque condition. The BLDCM and PMSM are controlled with custom-made small prototypes of the FSVSI and SSVSI, respectively. The current waveforms are measured using ACS712ELCTR-30A-T Hall effect-based linear current sensors from Allegro©. Also, the BLDCM speed is estimated with the aid of three built-in Hall effect-based position sensors using (1). The generated gate commands signals are fed to the FSVSI through isolated gate drive circuitry with A3120 gate drivers. All the control units including the proposed speed and current controllers as well as control of the PMSM are implemented in MATLAB/SIMULINK. The dSPACE1104 platform is used for controlling the HiL setup. The implemented controllers are compiled using MATLAB's CODER option and the built description file is used in dSPACE ControlDesk experiment software, which enables real-time control, monitoring, and data-logging, simultaneously. The current waveforms are recorded using Tektronix MSO5054 digital oscilloscope. The speed waveforms are first recorded as MATLAB's standard files and are then used for plotting in MATLAB. The sampling time of the description file, hysteresis controller, and MPC controller are set to 100μs. Detailed information on the HiL test setup and the BLDCM is provided in Table II. In the following subsection, the experimental results are provided and discussed.

TABLE II
Experimental Parameters

Parameter	Value
BLDCM	1.2kW, 72V hub motor
Loading Machine	1.5kW, 48V PMSM
Control Board	dSPACE1104 platform
Current Sensors	ACS712ELCTR-30A-T
T_s	100 μs
MPC horizons	N_p =2 , N_c = 1
Control band ε	0.5
Weighting Factors	δ = 0.7 , λ = 0.3
P	4
J	0.0012 kg.m^2
B	0.001 N.m.s

B. Experimental Results

The performance of the proposed control scheme is investigated through several experiments under different operating conditions. In Fig. 9, the steady-state three-phase BLDCM currents, three-phase Hall effect signals, as well as the switching signals of the FSVSI under load torque of 2 Nm and rotational speed of 600 rpm are shown. As seen, the quasi-square current waveforms are successfully constructed using the current controller based on hysteresis control. It is evident that during the rest modes of Phase C (modes 2 and 5), the controller suitably adjusts the current around almost zero. Overall, Fig. 9 shows that based on Fig. 1 and switching sequences of Table I, the waveforms are constructed exactly as expected. The controller performance can further be improved by reducing the control band, which would be obtained at the cost of slightly higher switching frequency and losses. Fig. 10 shows the experimental waveforms of the proposed method in generator mode. Similar to the motor mode, the quasi-square current waveforms are successfully constructed in the generator mode using the proposed strategy of Table I. In the conventional

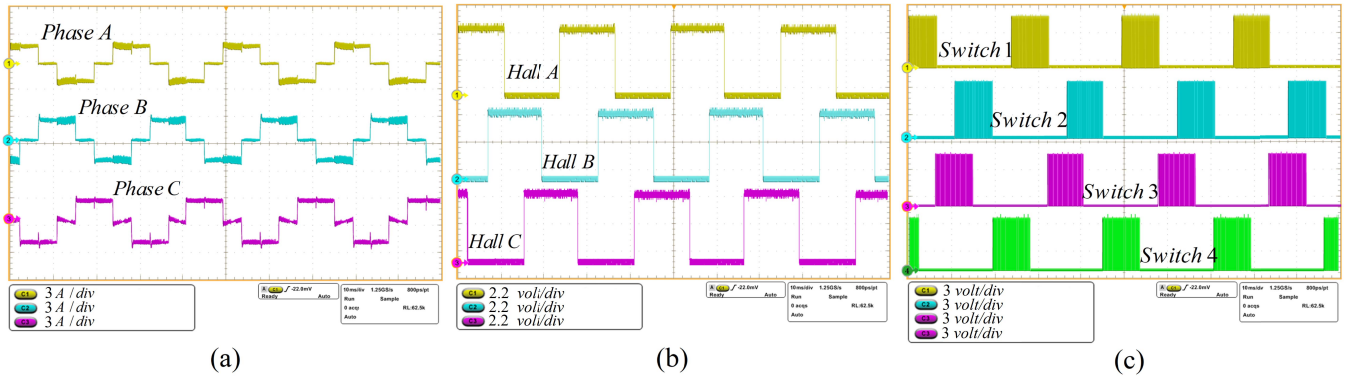

Fig. 9. Experimental waveforms in the steady-state conditions when the BLDCM works in the motor mode and is loaded by 2 Nm of the rated load torque and rotates at 600rpm. (a) Three-phase BLDCM phase currents. (b) Three-phase Hall effect signals. (c) Switching signals S_1 to S_4.

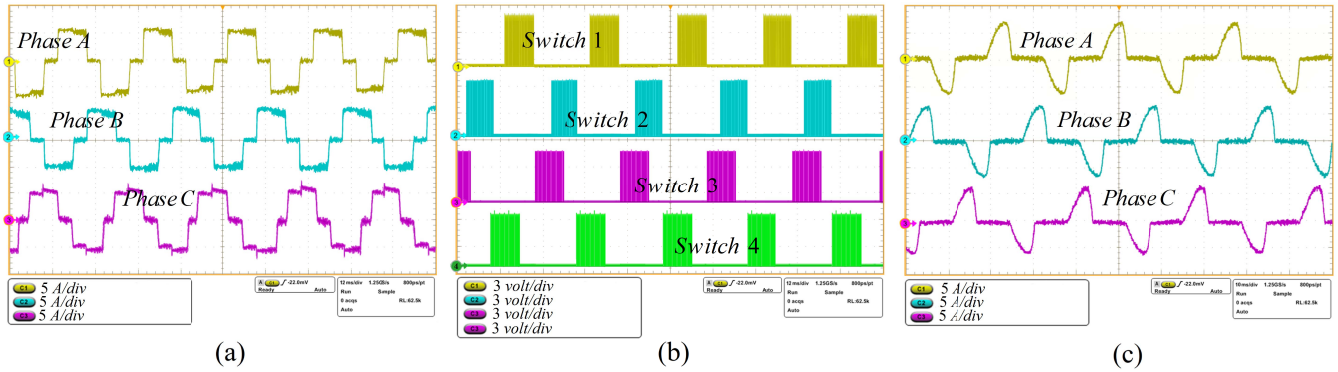

Fig. 10. Experimental waveforms in the steady-state conditions when the BLDCM operates in the generator mode and rotates at 600rpm. (a) Three-phase BLDCM phase currents with using the proposed switching strategy. (b) The switching signals S_1 to S_4 in the same time interval of Fig. 9(a). (c) Three-phase BLDCM phase currents without using the proposed switching strategy.

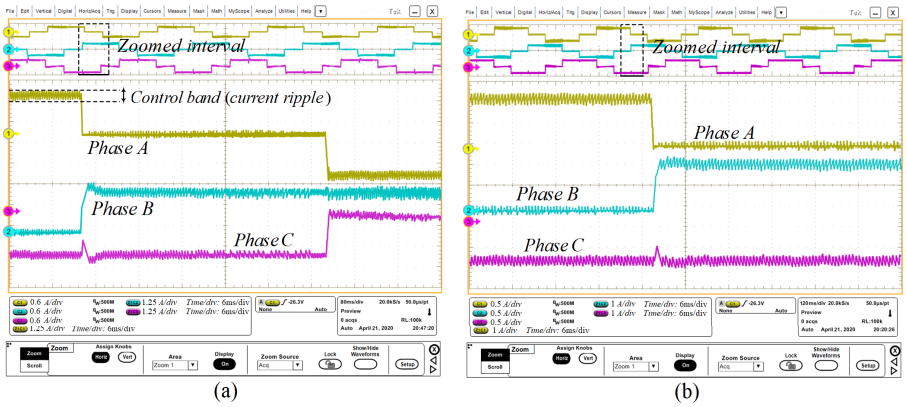

Fig. 11. Zoomed three-phase current waveforms of the BLDCM at different rotational speeds. (a) 1200 rpm (b) 800 rpm.

scheme, the energy released during the generator mode can be transmitted to the DC-link through conduction of anti-parallel diodes of the IGBTS, which will result in the current waveforms of Fig. 10(c). However, due to the trapezoidal back-EMFs of the BLDCM, such current waveforms will cause pulsative regenerative (braking) torque, which is not desirable. Using the proposed control strategy, a relatively smooth torque can be guaranteed during both the motor and generator modes. Fig. 11 shows the zoomed three-phase current waveforms under two different rotational speeds of 1200rpm and 800 rpm. It is evident that in both cases, the phase currents are appropriately regulated within the chosen control band of 0.5A. The current (torque) ripple can further be reduced by decreasing the band of the hysteresis controller. However, decreasing the controller band causes the phase current to reach the upper and lower bounds, more frequently. Therefore, a very low controller band can cause the excessive generation of heat due to the switching losses of the IGBTs. In practice, the band of the current controller must always be limited to a suitable value. In Figs. 12 and 13, the dynamic performances of the

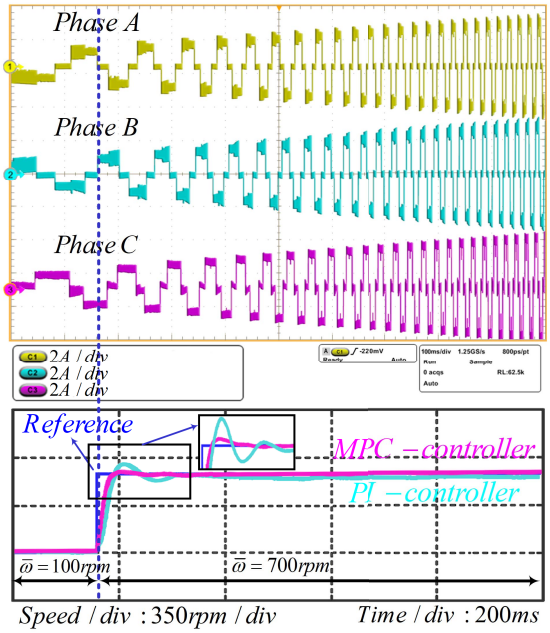

Fig. 12. Experimental waveforms under the speed change condition when the BLDCM speed is increased from 100rpm to 600rpm in a stepwise manner. Upper: Three-phase BLDCM phase currents. Lower: Speed responses of the proposed MPC-based controller and PI controller.

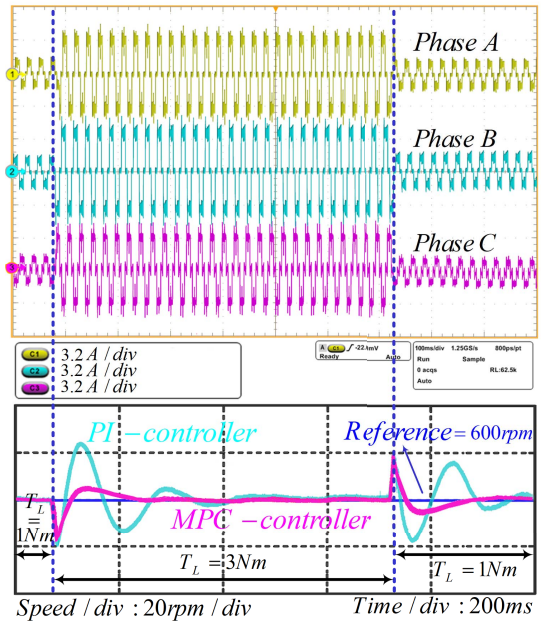

Fig. 13. Experimental waveforms under sudden step load changes from 1Nm to 3Nm and vice versa. Upper: Three-phase BLDCM phase currents. Lower: Speed responses of the proposed MPC-based controller and PI controller.

proposed control scheme under transient speed change and transient load change conditions are shown. Fig. 12 shows the three-phase BLDCM phase currents and speed response when the BLDCM reference speed is increased from 100 rpm to 700 rpm in a stepwise manner. The current waveforms indicate the proper construction of the quasi-square current waveforms during the speed change conditions. The speed response of the proposed MPC-based speed controller, as well as the comparison with the traditional PI controller, are shown in the lower

TABLE III
COMPARISON BETWEEN DIFFERENT SPEED CONTROL METHODS

	Rise time	Settling time*	Overshoot	Error**
PI [5]	~25 m.s.	~170 m.s.	~87 rpm	~ 10 rpm
Fuzzy-Logic [18]	~120 m.s.	~150 m.s.	<5 rpm	< 1 rpm
MPC (proposed)	~20 m.s.	~30 m.s.	<5 rpm	< 1 rpm

* 5% criterion (when speed settles within 5% of the steady-state value) * Steady-state error

plot of Fig. 12. The PI is tuned to provide its best performance in terms of transient overshoot, settling time, as well as the steady-state speed tracking error. The results suggest that the MPC and PI controllers both achieve a sufficiently small rise time below 20 milliseconds. However, the transient speed response with the PI controller shows a relatively big overshoot reaching 50 rpm, which is not acceptable for the FSVSI-based BLDCM application. On the other hand, the speed overshoot with the MPC controller is favorably below 4 rpm making it superior to its counterpart. Also, the steady-state speed tracking error of <0.5rpm is achieved with the MPC controller, which is very advantageous in comparison with the steady-state error of the PI controller obtained about 3 rpm. Although the PI controller can potentially achieve a lower tracking error by increasing the coefficient of the integrator term this will give rise to the speed settling time, which is not desirable. Fig. 13 shows the experimental waveforms when two successive sudden step changes in the load torque from 1Nm to 3Nm and vice-versa take place. It is evident that before the occurrence of the load change both of the controllers have successfully tracked the reference speed 600rpm. However, the BLDCM speed experiences a rapid decrease by about 20rpm when the load torque is suddenly increased to 3Nm. The speed response with the MPC controller shows that the speed successfully converges on the speed setpoint while it experiences a small overshoot with about 4 rpm. On the other hand, the speed response with the PI controller experiences two overshoot and undershoot of about 25 rpm and 15rpm, respectively. Besides, the settling time of the MPC-controller is significantly lower than that of the PI controller. Likewise, during the second load torque change condition when the torque is suddenly reduced from 3Nm to 1Nm., the BLDCM speed suddenly diverges from its setpoint; however, the reference speed is smoothly recovered using the proposed MPC-based control scheme. Similar to the first load change event, the speed response of the MPC excels the response of the PI controller in terms of the settling time and overshoot. Overall, the results demonstrate that the proposed method performs as designed and provides satisfactory performance characteristics, which makes it a rational candidate for low and medium-power BLDCM applications, where a limited amount of current harmonics can be tolerated. A few potential applications include but are not limited to the fan, pump, compressor, and spindle drives, small electric vehicles, bikes, and scooters.

V. COMPARISON WITH SIMILAR CONTROL METHODS

In this section, the performance of the proposed MPC-based control scheme is compared with the fuzzy-logic-based

controller and PI controller in terms of the rise time, settling time (5% criterion), overshoot, and steady-state speed tracking error. The comparative tests are carried out by computer simulations using MATLAB/SIMULINK software. The obtained results are summarized in Table III. The results clearly show the superiority of the proposed speed control method against the conventional PI controller. The proposed MPC-based controller also outperforms the fuzzy-logic-based controller in terms of the rise time and settling time.

VI. Concluding Remarks

In this paper, a new FSVSI-based BLDCM drive system is proposed. The adopted control scheme mainly comprises an inner current control loop based on the hysteresis controller and an outer speed control loop realized by MPC. The quasi-square current waveforms of the BLDCM are successfully formed using efficient switching strategies for both motor and generator operation modes. In comparison with the PI-based speed controller, the proposed speed controller improves the performance in terms of the overshoots, undershoots, as well as the setting time, thereby reducing the stresses on the weak FSVSI-based BLDCM drive. The MPC controller is realized by solving the relevant CF in an offline manner, which makes its implementation as simple as a PI controller. The proposed BLDCM drive scheme would be a very suitable choice for BLDCM drives that require high performance but very low investment cost.

Acknowledgment

The authors sincerely appreciate the financial support of Irans National Elites Foundation for carrying out this research.

References

[1] F. Naseri, E. Farjah, and T. Ghanbari, "An efficient regenerative braking system based on battery/supercapacitor for electric, hybrid, and plug-in hybrid electric vehicles with BLDC motor," *IEEE Trans. Veh. Technol.*, vol. 66, no. 5, pp. 3724–3738, May 2017.

[2] A. Loria, "Robust linear control of (chaotic) permanent-magnet synchronous motors with uncertainties," *IEEE Trans. Circuits Syst. I, Reg. Papers*, vol. 56, no. 9, pp. 2109–2122, Sep. 2009.

[3] F. Naseri, E. Farjah, Z. Kazemi, E. Schaltz, T. Ghanbari, and J.-L. Schanen, "Dynamic stabilization of DC traction systems using a supercapacitor-based active stabilizer with model predictive control," *IEEE Trans. Transport. Electrific.*, vol. 6, no. 1, pp. 228–240, Mar. 2020.

[4] B. K. Lee and M. Ehsani, "Advanced BLDC motor drive for low cost and high performance propulsion system in electric and hybrid vehicles," in *Proc. IEEE Int. Electr. Mach. Drives Conf.*, Jun. 2001, pp. 246–251.

[5] B.-K. Lee, T.-H. Kim, and M. Ehsani, "On the feasibility of four-switch three-phase BLDC motor drives for low cost commercial applications: Topology and control," *IEEE Trans. Power Electron.*, vol. 18, no. 1, pp. 164–172, Jan. 2003.

[6] B. K. Lee, T. H. Kim, and M. Ehsani, "On the feasibility of four-switch three-phase BLDC motor drives for low cost commercial applications: Topology and control," in *Proc. IEEE Appl. Power Electron. Conf. Expo.*, vol. 1, Mar. 2001, pp. 428–433.

[7] J. Kim, J. Hong, and K. Nam, "A current distortion compensation scheme for four-switch inverters," *IEEE Trans. Power Electron.*, vol. 24, no. 4, pp. 1032–1040, Apr. 2009.

[8] S.-H. Park, T.-S. Kim, S.-H. Ahn, and D.-S. Hyun, "A simple current control algorithm for torque ripple reduction of brushless DC motor using four-switch three-phase inverter," in *Proc. IEEE Conf. Power Electron. Spec.*, vol. 2, Jun. 2003, pp. 574–579.

[9] C. Zhu, Z. Zeng, and R. Zhao, "Comprehensive analysis and reduction of torque ripples in three-phase four-switch inverter-fed PMSM drives using space vector pulse-width modulation," *IEEE Trans. Power Electron.*, vol. 32, no. 7, pp. 5411–5424, Jul. 2017.

[10] Z. Zeng, C. Zhu, X. Jin, W. Shi, and R. Zhao, "Hybrid space vector modulation strategy for torque ripple minimization in three-phase four-switch inverter-fed PMSM drives," *IEEE Trans. Ind. Electron.*, vol. 64, no. 3, pp. 2122–2134, Mar. 2017.

[11] W. Li, S. Xuan, Q. Gao, and L. Luo, "Investigation of a four-switch four-leg inverter: Modulation, control, and application to an IPMSM drive," *IEEE Trans. Power Electron.*, vol. 34, no. 6, pp. 5655–5666, Jun. 2019.

[12] C. Xia, D. Wu, T. Shi, and W. Chen, "A current control scheme of brushless DC motors driven by four-switch three-phase inverters," *IEEE J. Emerg. Sel. Topics Power Electron.*, vol. 5, no. 1, pp. 547–558, Mar. 2017.

[13] S. B. Ozturk, W. C. Alexander, and H. A. Toliyat, "Direct torque control of four-switch brushless DC motor with non-sinusoidal back EMF," *IEEE Trans. Power Electron.*, vol. 25, no. 2, pp. 263–271, Feb. 2010.

[14] C. Xia, Z. Li, and T. Shi, "A control strategy for four-switch three-phase brushless DC motor using single current sensor," *IEEE Trans. Ind. Electron.*, vol. 56, no. 6, pp. 2058–2066, Jun. 2009.

[15] C.-T. Lin, C.-W. Hung, and C.-W. Liu, "Sensorless control for four-switch three-phase brushless DC motor drives," in *Proc. IEEE Ind. Appl. Conf., 41t IAS Annu. Meeting*, Oct. 2006, pp. 2048–2053.

[16] C.-T. Lin, C.-W. Hung, and C.-W. Liu, "Position sensorless control for four-switch three-phase brushless DC motor drives," *IEEE Trans. Power Electron.*, vol. 23, no. 1, pp. 438–444, Jan. 2008.

[17] A. H. Niasar, A. Vahedi, and H. Moghbelli, "A novel position sensorless control of a four-switch, brushless DC motor drive without phase shifter," *IEEE Trans. Power Electron.*, vol. 23, no. 6, pp. 3079–3087, Nov. 2008.

[18] M. N. Uddin, T. S. Radwan, and M. A. Rahman, "Fuzzy-logic-controller-based cost-effective four-switch three-phase inverter-fed IPM synchronous motor drive system," *IEEE Trans. Ind. Appl.*, vol. 42, no. 1, pp. 21–30, Jan. 2006.

[19] D. Sun, J. Su, C. Sun, and H. Nian, "A simplified MPFC with capacitor voltage offset suppression for the four-switch three-phase inverter-fed PMSM drive," *IEEE Trans. Ind. Electron.*, vol. 66, no. 10, pp. 7633–7642, Oct. 2019.

[20] W. Hua, W. Huang, and F. Yu, "Improved model-predictive-flux-control strategy for three-phase four-switch inverter-fed flux-reversal permanent magnet machine drives," *IET Electr. Power Appl.*, vol. 11, no. 5, pp. 717–728, May 2017.

[21] H. Ren and D. Liu, "Nonlinear feedback control of chaos in permanent magnet synchronous motor," *IEEE Trans. Circuits Syst. II, Exp. Briefs*, vol. 53, no. 1, pp. 45–50, Jan. 2006.

[22] H. Yan, J. Han, H. Zhang, X. Zhan, and Y. Wang, "Adaptive event-triggered predictive control for finite time microgrid," *IEEE Trans. Circuits Syst. I, Reg. Papers*, vol. 67, no. 3, pp. 1035–1044, Mar. 2020.

[23] R. Morfin-Magaña, J. J. Rico-Melgoza, F. Ornelas-Tellez, and F. Vasca, "Complementarity model of a photovoltaic power electronic system with model predictive control," *IEEE Trans. Circuits Syst. I, Reg. Papers*, vol. 66, no. 11, pp. 4402–4414, Nov. 2019.

[24] A. Mohammadi, H. Asadi, S. Mohamed, K. Nelson, and S. Nahavandi, "Optimizing model predictive control horizons using genetic algorithm for motion cueing algorithm," *Expert Syst. Appl.*, vol. 92, pp. 73–81, Feb. 2018.

[25] Z. Kazemi, A. A. Safavi, S. Pouresmaeeli, and F. Naseri, "A practical framework for implementing multivariate monitoring techniques into distributed control system," *Control Eng. Pract.*, vol. 82, pp. 118–129, Jan. 2019.

Farshid Naseri (Member, IEEE) received the B.Sc. degree in electrical engineering from the Shiraz University of Technology, Shiraz, Iran, in 2013, and the M.Sc. and Ph.D. degrees in power electronics from Shiraz University, Shiraz, Iran, in 2015 and 2019, respectively. In 2019, he joined the Electro-Mobility and Industrial Drives Research Program at the Department of Energy Technology, Aalborg, Denmark, as a Guest Researcher. Since 2020, he has been working as a Post-Doctoral Fellow with the Department of Electrical and Computer Engineering, Shiraz University. In his post-doctoral project, he is working on software design for vehicular battery management systems to fulfill the state estimation, balancing, and protection of the lithium-ion batteries. His current research interests include electric vehicles, battery and supercapacitor energy storage systems, and battery management systems.

Ebrahim Farjah (Member, IEEE) received the B.Sc. degree in electrical and electronics engineering from Shiraz University, Iran, in 1987, the M.Sc. degree in electrical power engineering from the Sharif University of Technology, Tehran, Iran, in 1989, and the Ph.D. degree in electrical engineering from the Grenoble Institute of Technology, Grenoble, France. He is currently a Professor with the Department of Electrical and Computer Engineering, Shiraz University. His research interests include power electronics, renewable energy, micro-grids, and power quality.

Erik Schaltz (Member, IEEE) received the M.Sc. and Ph.D. degrees in electrical engineering from the Department of Energy Technology, Aalborg University, Aalborg, Denmark, in 2005 and 2010, respectively. From 2009 to 2012, he was working as an Assistant Professor with the Department of Energy Technology, Aalborg University, where he is currently working as an Associate Professor. At the department, he is the Programme Leader of the research programme in e-mobility and industrial drives and the Vice Programme Leader of battery storage systems. His research interests include analysis, modeling, design, and control of power electronics, electric machines, energy storage devices, including batteries and ultracapacitors, fuel cells, hybrid electric vehicles, thermoelectric generators, reliability, and inductive power transfer systems.

Kaiyuan Lu (Member, IEEE) received the B.S. and M.S. degrees from Zhejiang University, Zhejiang, China, in 1997 and 2000, respectively, and the Ph.D. degree from Aalborg University, Denmark, in 2005, all in electrical engineering. In 2005, he became an Assistant Professor with the Department of Energy Technology, Aalborg University, where he has been an Associate Professor, since 2008. His research interests include the design of permanent magnet machines, finite element method analysis, and control of permanent magnet machines.

Nima Tashakor (Graduate Student Member, IEEE) received the B.Sc. degree in electrical power engineering from Isfahan University, Isfahan, Iran, in 2013, and the M.Sc. degree in electrical power engineering from Shiraz University, Shiraz, Iran, in 2015. He is currently pursuing the Ph.D. degree with the Technical University of Kaiserslautern, Germany.

His research field includes power electronics and energy storage systems with a focus on modular converters development and control. Furthermore, he investigates the application of machine learning in power electronics applications.